# Part II

# Application of the Model to the Problem of Interannual Variability of Martian Global Dust Storms

# Chapter 5 Introduction

Martian global dust storms are among the most stunning atmospheric phenomena in the solar system. During these events, intensified winds carry surface dust into the atmosphere and rapidly spread it over much of the planet. Micron-size dust particles suspended in the atmosphere obscure surface features on a global scale and dramatically alter thermal and dynamical structure of the atmosphere. Dust remains in the atmosphere for months before settling back to the surface. One of the most enigmatic properties of the martian climate is that GDSs have been observed to occur repeatedly but not every year. Here I present results of simulations of the interannual variability of martian GDSs with the LOM of global circulation described in Part I of the thesis.

## 5.1 Properties of the GDSs

Observations allow one to distinguish a number of characteristic properties of the martian GDSs. The GDSs seemingly result from an expansion and coalescence of several local dust storms (LDSs). The expansion proceeds in the east-west direction at first, followed by meridional spreading of dust into high southern latitudes and middle northern latitudes. The reason behind the rapid growth of GDSs appears to be a positive radiative-dynamic feedback that involves intensification of winds by heating due to atmospheric dust, and raising of more dust by intensified winds [ZBH+92]. The decay phase follows almost immediately after the expansion phase of the GDS. Opacity levels decrease exponentially [Con75, PCF+79, CPH89] to prestorm values, with the decay time of the order of 50 days [Con75, PCF+79]. The decay phase of the storm is consistent with the removal of micron-size particles by gravitational settling [Con75].

Several other attributes of GDSs merit detailed consideration here. They are

seasonality, location of origin and interannual variability. It will be shown that the LOM described in Part I is capable of reproducing most of these properties. Since the LOM is a longitudinally averaged model, the longitudinal spreading of the GDS during the growing phase cannot be reproduced by the LOM.

### 5.1.1 Seasonality

All of the observed GDSs and the largest LDSs have occurred during martian southern spring and summer [Zur82, ZM93] (Fig. 5.1). The beginning of the southern summer ($L_s = 270°$) currently almost coincides with the time of the perihelion passage ($L_s = 251°$). Thus, most theories of the GDSs attribute seasonal occurrence of the GDSs to the increase in solar heating of the surface and intensification of the global circulation around perihelion [HPB$^+$93]. On the other hand, seasonality may reflect the bias in observations of Mars, mentioned earlier.

### 5.1.2 Location of origin

The GDSs originate in the southern subtropical regions of Mars, the most common sites being Noachis-Hellespontus and Solis Planum-Argyre regions [Tho79, Mar74]. These areas feature high topographic slopes, which hints at the role of topographic winds in the generation of dust storms. Locations of origin of the GDSs are close to the latitude of the sub-solar point [Pet85], which suggests that solar heating of the surface is important in bringing dust into the atmosphere. The preferred origin of the GDSs in the southern subtropics may, at the same time, reflect the surface distribution of dust and/or of saltating sand grains [Pet81, KMZL92].

### 5.1.3 Interannual variability

Interannual variability is one of the most intriguing properties of the martian GDSs. The GDSs were observed to occur repeatedly, but not every year [Mar84, ZM93, KMZL92] (Fig. 5.2). Even though large LDSs probably occur every year [Zur82], they do not always coalesce into a GDS. There is no apparent event that triggers

the GDSs. Atmospheric processes on Mars occur over time scales that are much shorter than the martian year, the longest one being the dust fallout time $t_d \sim 1/10$ martian year. Hence, there is no long-term memory in the system, while on Earth it is provided by oceanic heat storage, vegetation, sea ice cover, and so on.

## 5.2 Hypotheses for the Cause of Interannual Variability

Several theories of the martian GDSs has been proposed [GG73, LZP73, LTGB85, Sch83, Hab86, ZBH+92]. However, only a few of them address interannual variability. The LOM developed in Part I is suitable for testing theories of the interannual variability of the GDSs. However, rather than testing every hypothesis, it is convenient to assign them to two different classes of hypotheses: those with intrinsic and those with extrinsic irregularity. Results of simulations with the LOM reported in Chapters 6 and 7 suggest that the interannual variability is more readily explained by the extrinsic irregularity.

### 5.2.1 Intrinsic and extrinsic irregularity

Hypotheses of the intrinsic irregularity would imply that the atmosphere-dust system is a chaotic system and the interannual variability is a manifestation of this chaotic behavior [Hab86, ZH89, ZBH+92, IL93]. In [ZH89, IL93, ZBH+92] it was suggested that the martian atmosphere is a chaotic dynamical system, where nonlinear interactions between components can lead to different states of the system. The same hypothesis has been proposed to explain the interannual variability of the El Niño-Southern Oscillation phenomenon [TSCJ94].

On the other hand, hypotheses of the extrinsic irregularity would imply that the variability is caused by random forcing originating outside the atmosphere-dust system [Sch83, LTGB85, Hab86]. When the forcing exceeds a critical value, a GDS occurs. In [Sch83, LTGB85] it was suggested that small perturbations of the state of

the climate system could push it into a regime with or without a GDS. In [Sch83], global expansion of the Hadley cell, which was interpreted as a start of a GDS, occurred when parameterized diabatic heating exceeded some critical value. Amplification of the Hadley circulation by relatively small amounts of atmospheric dust [PHSL90] could thus lead to a genesis of a GDS. The seemingly random occurrence of the LDSs or redistribution of dust in the background haze could thus introduce interannual variability into the occurrence of the GDSs.

The role of the background dust haze in producing the interannual variability was also considered in [Hab86]. It was suggested that the dust transported to the NH during the GDS of the previous year is raised locally the following year and creates a background haze. Increased solar heating of the NH weakens the global cross-equatorial Hadley cell that develops during southern summer, thus preventing occurrence of a GDS. The dust may then be redistributed, so that GDSs are possible in subsequent years. The interannual variability in this model could result from two factors. First, it may result from fluctuations in the NH dust haze. If the haze is dense enough, a GDS will not occur, and visa versa. The interannual variability will thus have a random component, due to the stochastic nature of the processes that determine the opacity of the NH dust haze. Second, the interannual variability may be a consequence of the redistribution of dust between the hemispheres, so there are different amounts of dust available for lifting in NH every year. In this case the variability depends on the properties of the dust storms (i.e., how much dust is transported and where it is deposited). Hence, [Hab86] can be included in both classes since both random and deterministic causes for the interannual variability were suggested.

## 5.3 Modeling Attempts

Previous attempts to simulate the GDSs employed interactive 2D models [HLP82, MHTP93] or full 3D GCMs with a prescribed dust source and fixed dust distributions [MI80, PHSL90, HPB$^+$93, MPH$^+$95]. Simulations with a prescribed dust source

produce results that are in good agreement with available observations. However, no attempts to simulate the interannual variability with the GCMs or 2D models have been published. The simulations of the interannual variability of the GDSs with the LOM presented in the following chapters represent the first attempt of this sort.

Figure 5.1: Optical depth of the martian atmosphere for the first year of VLs observations. Arrows mark the $L_s$ values of the onset of historical GDSs (denoted by the year of occurrence) (figure adopted from [GLLT92]).

Figure 5.2: Timeline of the detection of LDSs and GDSs. Earth dates are indicated at the top, and perihelion (and thus Mars year) at the bottom of the dust-storm timeline. The second timeline indicates periods of photographic coverage of Mars, defined in terms of percentage of $L_s$ degrees that photographs were taken. The third timeline indicates the apparent size of Mars, as seen from Earth, on scale of 0 to 30 seconds of arc (figure adopted from [KMZL92]).

# Chapter 6 Behavior of the LOM with Deterministic Forcing

## 6.1 Behavior of the LOM with Interactive Dust Source

To test hypotheses of the intrinsic irregularity of the martian atmosphere-dust system, the LOM was run with the set of parameters used in Chapter 2 and an interactive dust source. The Rayleigh friction coefficient $r$ was kept constant in all simulations. No interannual variability was found for a wide range of parameter values. Figure 6.1 shows a time series of model variables for the parameters $1/r = 5$ sols, $t_r = 2$ sols, $T^e_{av} = 195$ K, $T^e_{ns} = 15$ K, $T^e_v = -35$ K, $T^e_{em} = 2$ K, $U^*_t = 1$, $s_0 = 0.5$ and PSD1 (Fig. 2.6). The upper panel shows zonal winds $u_s$ (dashed) and $u_a$ (solid) in m/s. The second panel from above shows the mean stream functions $\psi_s$ (solid) and $\psi_a$ (dashed) in units of $10^8$ kg $s^{-1}$. The third panel from above shows temperatures $T_{ns}$ (solid),$-T_v$ (dashed), $T_{em}$ (dotted) and $c_4 T_{av}$ (dashed-dotted) in Kelvins. The lower panel shows optical depths in SH (solid) and NH (dashed). The horizontal axis in all plots represent time measured in martian years (88775 seconds) from perihelion ($L_s = 251°$). The behavior of the system is periodic in this case. For the chosen values of the threshold friction speed $U^*_t$ and the amplitude of the dust source $s_0$, GDSs occur every year in the SH around perihelion. During the GDS atmospheric temperature and wind fields change dramatically. The asymmetric part of the zonal winds $u_a$ increases by a factor of 2.5, while the symmetric part $u_s$ decreases to zero. This translates into an increase of the zonal jets, consistent with the GCM simulations of the dust storms [MPH+95]. The intensity of the meridional circulation approximately doubles, which is also consistent with the GCM modeling. The temperature lapse rate

decreases in response to warming of the upper layers of the atmosphere by dust. The hemispheric temperature difference $T_{ns}$ increases, as well as the average temperature of the atmosphere $T_{av}$. The simulated GDSs exhibit the general properties of the observed GDSs, except for the interannual variability.

Variations of the model parameters do not produce interannual variability. Figure 6.2 shows a simulation with the same parameter values as above, but with the amplitude of the source increased to $s_0 = 3.5$. The solutions are periodic. The GDSs are much more intense in this case, with the maximum dust optical depth in the SH reaching 16 at the peak of the storm. By comparing Fig. 6.1 and Fig. 6.2, it can be concluded that the maximum optical depths in both hemispheres scale approximately linearly with the value of $s_0$, other parameters being equal. The intensity of the meridional circulation also increases, although the zonal winds and the temperature fields are roughly the same as in Fig. 6.1. The duration of the increase of the meridional circulation is quite short – $\sim 3 - 5$ sols, compared to the duration of the GDS $\sim 100$ sols (time before opacity drops below 1).

Lowering the threshold friction speed $U_t^*$ below 1 leads to occurrences of the dust storms in both hemispheres. Figure 6.3 shows results of the simulations with $U_t^* = 0.5$ and $s_0 = 0.5$. The behavior of the system is periodic. The atmosphere remains dusty throughout the year, with maximum dustiness developing around aphelion and perihelion, which correspond to northern and southern summer, respectively. Maximum optical depth during a GDS is larger in the SH since the circulation and the dust source are stronger during southern summer.

Occurrences of the GDSs in the NH contradict observations. However, even if the interactive dust source is turned off in the NH, the system continues to behave periodically, as shown on Fig. 6.4. One GDS develops every year in the SH at the onset of the spring. The durations of the storms are much longer than that of the observed ones. An interesting feature of this simulation is the occurrence of two local maxima around perihelion in the time series of the zonal winds, stream function and hemispheric temperature difference $T_{ns}$. The first maximum occures shortly after the onset of the GDS. As the vertical temperature gradient decreases, the atmosphere be-

comes more stable and the intensity of the meridional circulation decreases. The dust is transported to the NH, and the hemispheric temperature difference and the zonal winds decrease as well. The second maximum occurs at perihelion, when the stream function, the zonal winds and the hemispheric temperature difference reach their seasonal maxima. An observer limited to observations of temperature and global winds would probably interpret these data as being consistent with two GDSs, occurring before and after perihelion.

Increasing the threshold friction speed $U_t^*$ above some critical value leads to cessation of occurrence of the GDSs. For the model parameter values used in the above simulations, this critical value of $U_t^*$ is 1.07.

## 6.2 Dust Source with Constant Component

Dust is present in various quantities in the martian atmosphere even during the periods without GDSs [CPH89, SL99, FPM97]. Various mechanisms have been proposed for raising dust when the background global winds are weak [GLLT92]. They include: dust devils, dust fountaining by desorbed $CO_2$ and $H_2O$, clumping of fine grains into larger aggregates more easily moved by winds, and others. Without considering the details of each mechanism, these alternative sources of dust were included in the LOM in the form of a dust source independent of the global winds. In the simulations presented in this section the independent dust source is assumed to be steady in time with the same intensity in each hemisphere. The results are similar to the results of the previous section in that no interannual variability was found.

Figure 6.5 illustrates the behavior of the LOM with constant sources in both hemispheres and suppressed interactive source. The intensity of the dust source in the SH, $s_s$, is equal to the intensity of the dust source in the NH, $s_n$, and is equal to 0.15. The hemispheric optical depths of the resultant background haze vary seasonally from 0.15 to $\sim 0.3$. Summer hemisphere is always dustier as the lower level meridional winds transport dust from the winter hemisphere into the summer hemisphere. In a given hemisphere, summer is the dustiest season for the same reason. This contradicts

the observations by VLs [CPH89] that indicate that the atmosphere was clearer in NH during summer. Apparently, the representation of the alternative dust sources by a constant source is too simple, and in reality the intensity of these sources may be seasonally variable.

Figure 6.6 shows the results of the LOM simulations with an interactive dust source and constant dust sources in both hemispheres. The dust source parameters are: $U_t^* = 1.1$, $s_0 = 0.5$, $s_n = s_s = 0.1$. The addition of the constant sources produces background dust haze in both hemispheres, but otherwise does not change the behavior of the system, which is periodic.

## 6.3 Conclusions

The results shown in this chapter suggest that the interannual variability of the GDSs on Mars cannot be explained by inherent variability of the martian atmosphere-dust system. Results of Chapter 3 suggest that the martian atmosphere is not a chaotic system. The residence time of dust in the atmosphere is too short to affect the state of the atmosphere in the subsequent year. The effect of the background dust haze on the atmosphere is also inadequate to produce the needed variability, at least in the context of the LOM. Some small scale processes, such as trapping of dust in craters or "shielding" by rocks, may account for the interannual variability, but they cannot be incorporated directly into the LOM. Instead, the effects of such processes could be viewed as noise added to some model parameters, for instance, to the threshold friction speed $U_t^*$. The effect of the stochastic forcing on the LOM is the concern of the next chapter.

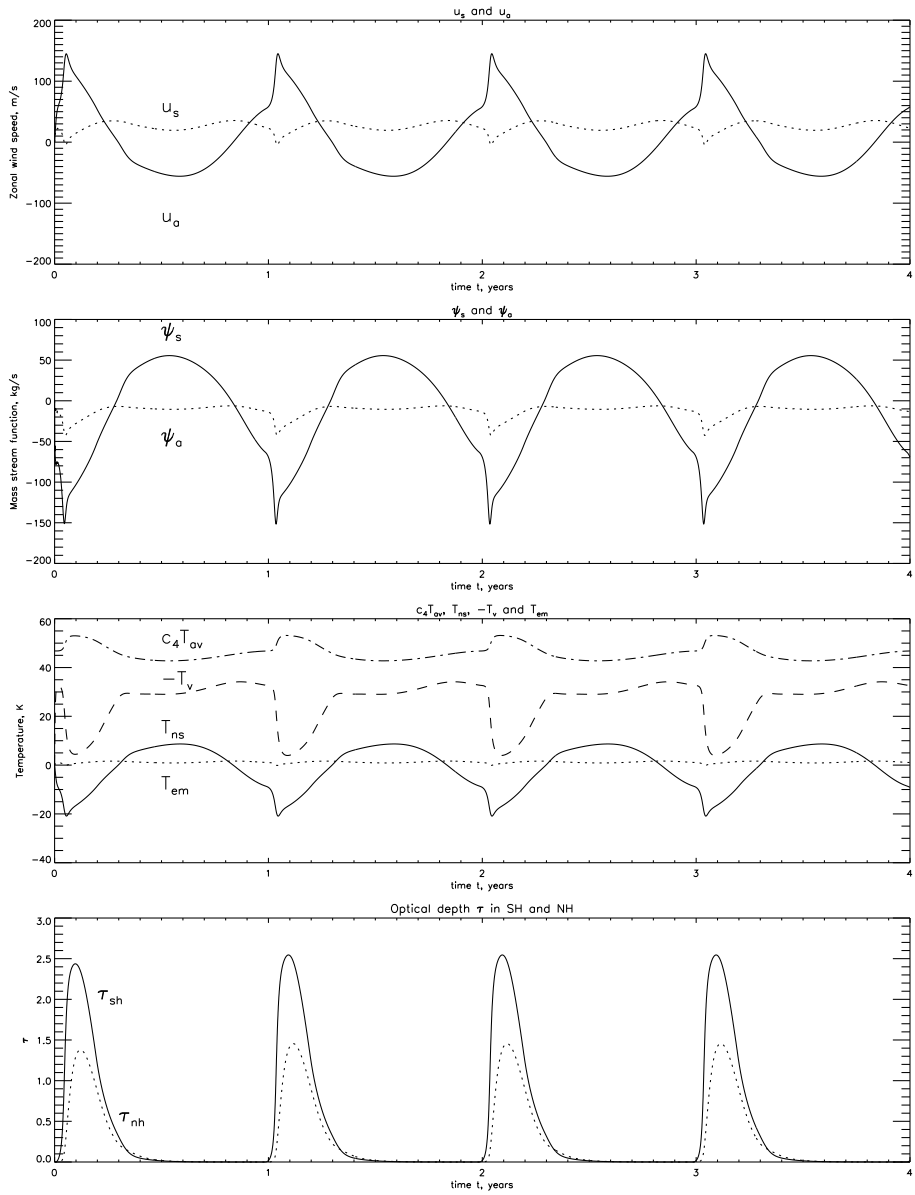


Figure 6.1: Time series of the LOM variables for the run with interactive dust source. Parameters of the model are the same as in Chapter 2, threshold friction speed $U_t^* = 1$, amplitude of the dust source $s_0 = 0.5$.

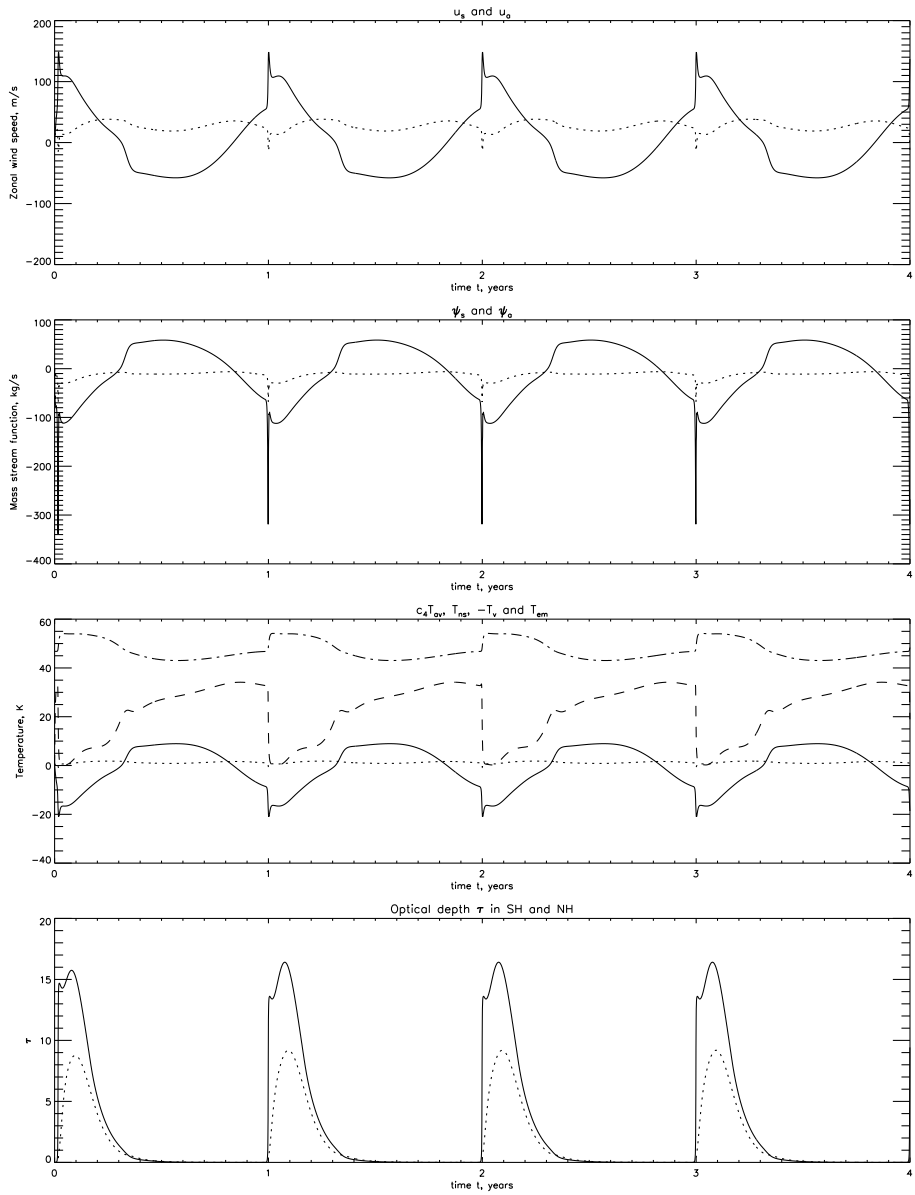


Figure 6.2: Same as Fig. 6.1, but with $s_0 = 3.5$.

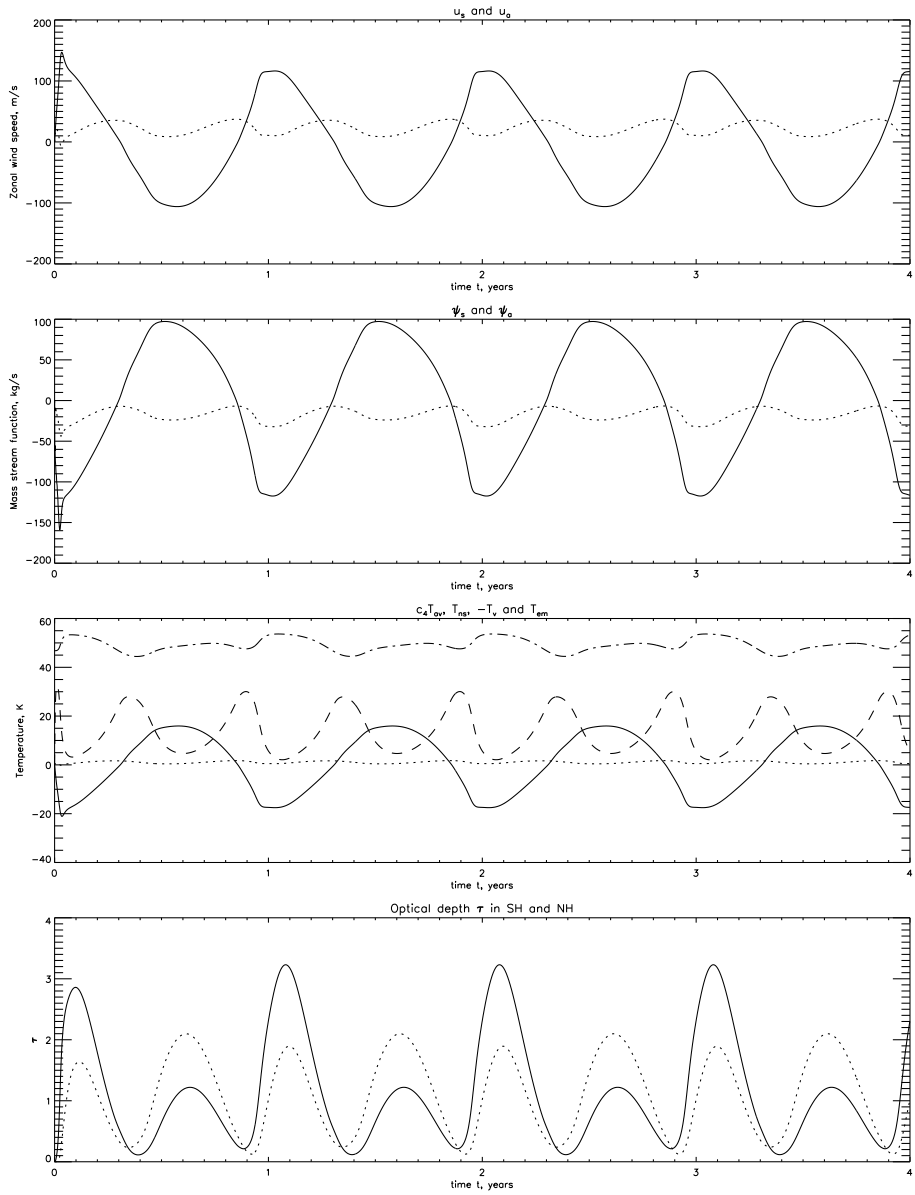


Figure 6.3: Same as Fig. 6.1, but with $U_t^* = 0.5$ and $s_0 = 0.5$.

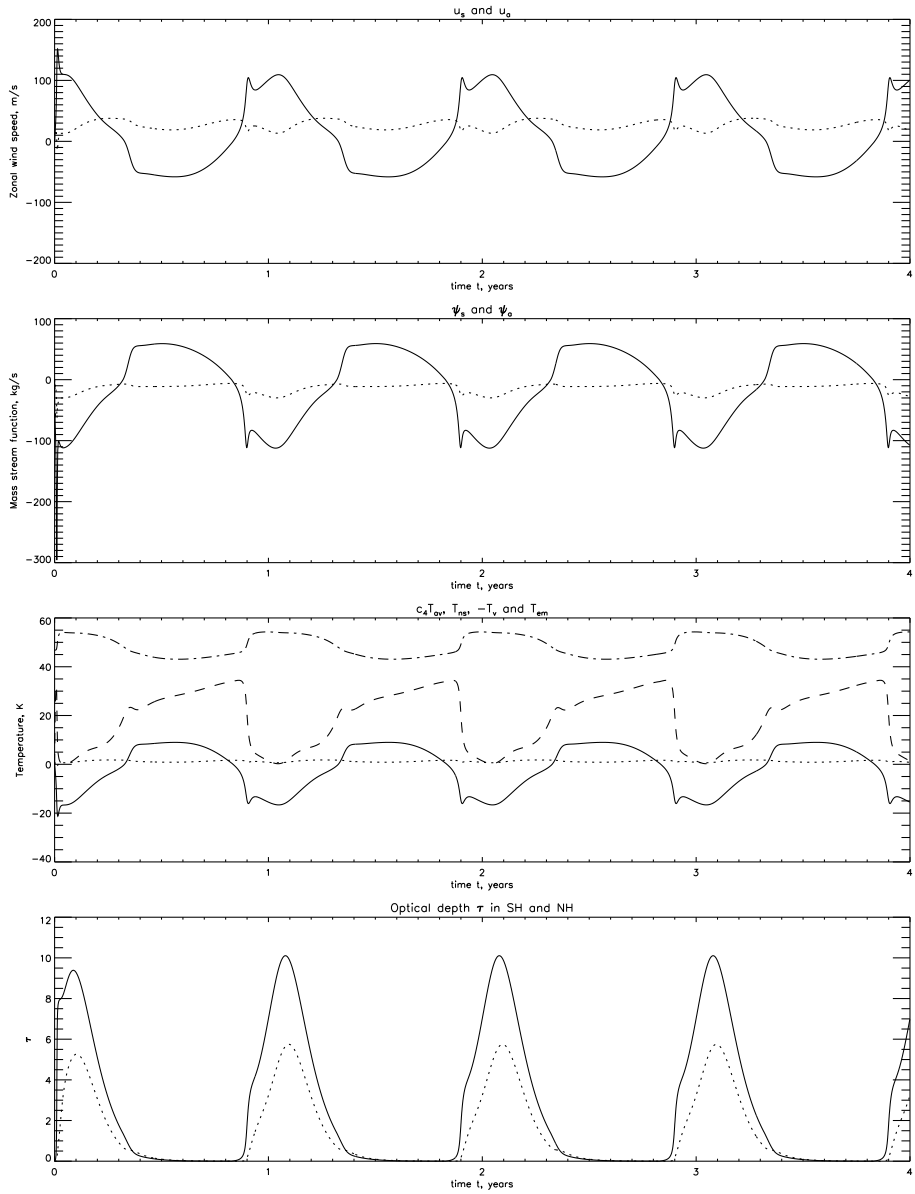


Figure 6.4: Same as Fig. 6.1, but with $U_t^* = 0.1$ and $s_0 = 2$ and GDS in NH suppressed.

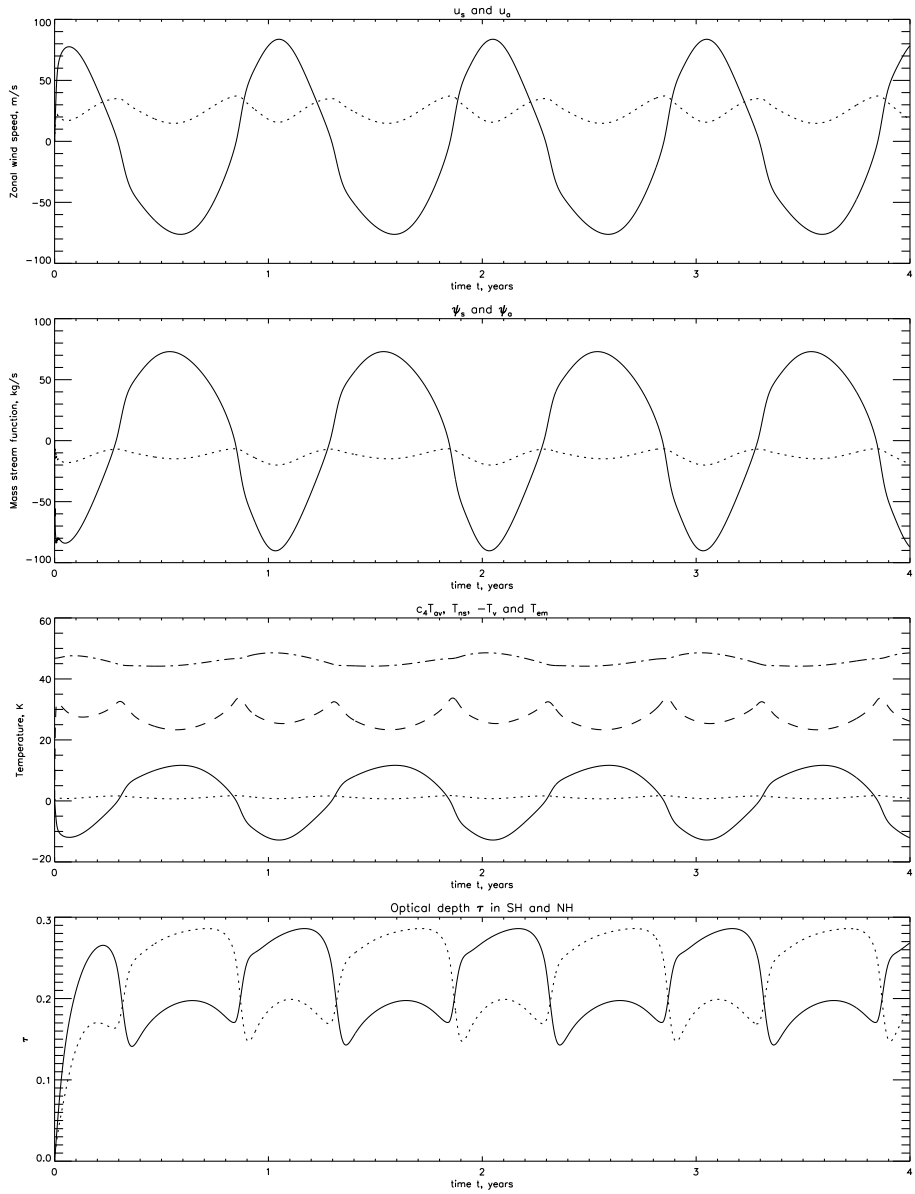


Figure 6.5: Same as Fig. 6.1, but for constant dust sources in both hemispheres, $s_n = s_s = 0.15$, and suppressed interactive source, $s_0 = 0$.

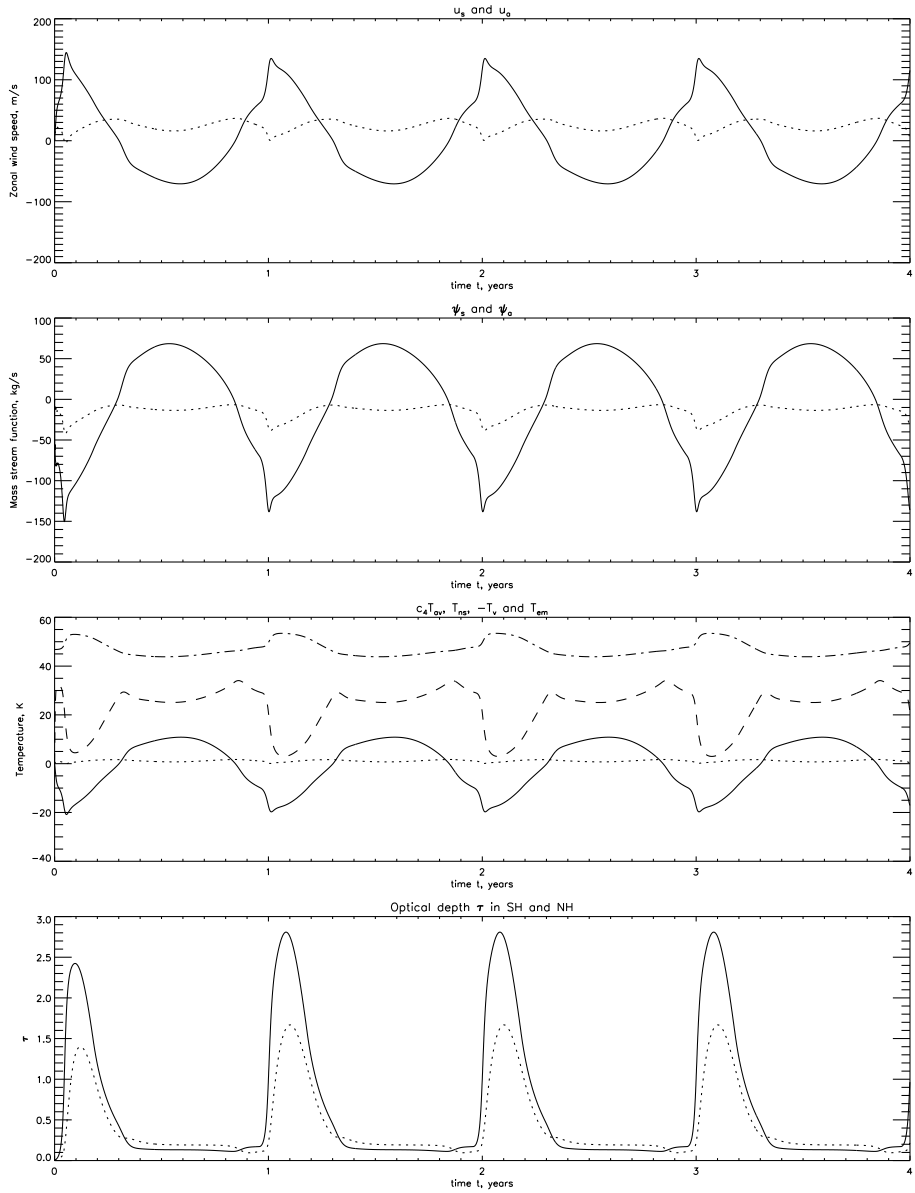


Figure 6.6: Same as Fig. 6.1, but for interactive dust source with constant component in both hemispheres, $s_n = s_s = 0.1$, $U_t^* = 1.1$, $s_0 = 0.5$.